

Particle-core study of halo dynamics in periodic-focusing channels

Tai-Sen F. Wang

MS H808, Los Alamos National Laboratory, Los Alamos, New Mexico 87545

(Received 4 August 1999)

This paper reports on an approach to investigate the dynamics of halo particles in mismatched charged-particle beams propagating through periodic-focusing channels using the particle-core model. The proposed method employs canonical transformations to minimize, in new phase-space variables, the flutter due to the periodic focusing to allow making stroboscopic plots. Applying this method, we find that in periodic-focusing systems, certain particles initially not in the halo region can be brought into resonance with the core oscillation to become halo particles.

PACS number(s): 41.85.-p, 29.17.+w, 29.27.Bd

I. INTRODUCTION

The particle-core model has provided insight of the dynamics of particles in the beam halo of a mismatched beam propagating through an axisymmetric uniform-focusing channel [1–12]. However, to date, only limited progress has been made in applying the same model to a beam propagating through a periodic-focusing channel [11]. The main obstacle stems from the flutter in the beam envelope and in the particle orbit introduced by the focusing. Owing to this flutter, the dimension of a Poincaré section made by strobing a particle's phase space is usually higher than two [13]. One then has to slice the phase space or to project the higher-dimensional Poincaré "plot" onto a two-dimensional plane in order to study the particle dynamics. The former approach is complicated by the searching for suitable phase-space slices, while the latter approach may result in a plot with few features to be deciphered. In this paper we will show that by using proper canonical transformations and strobing, the flutter due to the periodic focusing can be minimized in the new phase-space variables so that the primary resonance between the particle and the core is manifested in the projected stroboscopic plots. This method is applicable to a wide range of parameter values without using a smooth approximation, and it is not limited by the constraint that the frequency of core oscillation need be commensurable with that of the transverse focusing. Using this method, we find that the periodic focusing can be a possible mechanism for halo formation in a mismatched beam. For brevity, we will omit discussion of chaotic motion and stability of the core oscillation.

II. PARTICLE-CORE MODEL

We consider a test particle and a continuous beam (the core) propagating in a periodic-focusing channel with a speed v in the axial direction, the z direction. Particles are focused in the transverse direction by a linear force that varies in the z direction according to $GF(kz)$, where G is the maximal gradient of the focusing (or defocusing) strength, $F(kz)$ is a periodic function of z , k is the wave number of the periodicity, and the maximum of $|F(kz)|$ is normalized to unity. The particles in the core are assumed to follow the Kapchinskij and Vladimirkij (KV) [14] distribution in transverse phase space.

We discuss the axisymmetric case first. The dimensionless equations for the beam envelope and the transverse motion of the test particle are

$$\frac{d^2X}{d\tau^2} + Q^2XF(\tau) - \frac{\eta}{X} - \frac{1}{X^3} = 0, \quad (1)$$

and

$$\frac{d^2x}{d\tau^2} - \frac{L^2}{x^3} + Q^2xF(\tau) = \begin{cases} \eta x/X^2 & \text{for } x \leq X \\ \eta/x & \text{for } x > X, \end{cases} \quad (2)$$

respectively, where $X = X_r\sqrt{k/\epsilon}$, $x = x_r\sqrt{k/\epsilon}$, $\tau = kz$, X_r is the beam envelope, x_r is the transverse displacement of the particle from the symmetry axis of the system, ϵ is the beam emittance, $L = L_r/(m_0\gamma v\epsilon)$, $\eta = qI/(2\pi\epsilon_0 m_0\gamma^3 v^3 k\epsilon)$, $Q^2 = qG/(m_0\gamma v^2 k^2)$, q and m_0 are the charge and the rest mass of a beam particle, respectively, γ is the relativistic mass factor, I is the beam current, ϵ_0 is the permittivity of free space, and L_r is the angular momentum of the test particle about the z axis. Introducing a new variable $u_e = X/X_m$ and a new time s defined by $ds = d\tau/X_m^2$, we can rewrite Eq. (1) as

$$\frac{d^2u_e}{ds^2} + u_e - \frac{1}{u_e^3} = \eta X_m^2 \left(\frac{1}{u_e} - u_e \right), \quad (3)$$

where X_m is the envelope of the matched core defined by the condition $X_m(\tau) = X_m(\tau + 2\pi)$. It should be noted that the form of Eq. (3) will remain the same if X_m were any solution to Eq. (1). Choosing $w_e = du_e/ds$ as the conjugate variable of u_e , we can prove that the change of variables here is in fact a canonical transformation. We remark that, instead of the focusing function F , it is X_m that enters into Eq. (3). Also, the flutter due to the periodic focusing which is only a fraction of X_m is now in a term proportional to the beam current. Hence in the integrated solutions, the flutter in u_e is substantially smaller than that in X as can be seen in both perturbation calculations and numerical solutions. When $I = 0$, the flutter in u_e is suppressed completely. Next, using the time variable ψ defined by $d\psi = d\tau/X^2$, as well as a set of conjugate variables

$$(u, w) = \left(\frac{x}{X}, \frac{du}{d\psi} \right) = \left(\frac{x}{X}, X \frac{dx}{d\tau} - x \frac{dX}{d\tau} \right), \quad (4)$$

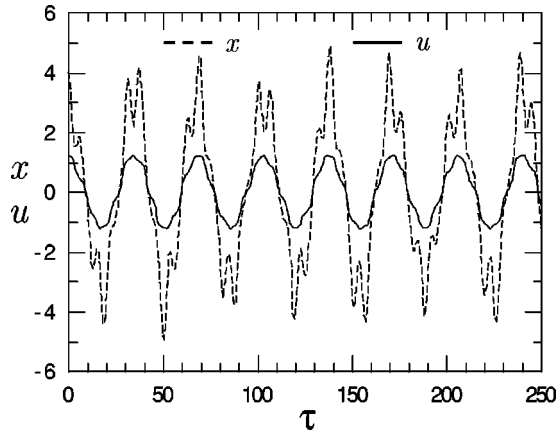


FIG. 1. Orbit x and quantity u of a particle in a mismatched beam propagating in a periodic-focusing channel. The parameter values are described in the text.

one can infer from Eq. (2) a Hamiltonian:

$$H_p = \frac{L^2}{2u^2} + \frac{u^2 + w^2}{2} - \frac{\eta X^2}{2} \Theta(u-1)(\ln u^2 + 1 - u^2), \quad (5)$$

where $\Theta(x)$ is the Heaviside step function. The generating function of the corresponding canonical transformation is $f_2(x, w) = x[w + (x/2)(dX/d\tau)]/X$. The flutter is reduced in u and w for the similar reasons discussed in connection with u_e . Note that one can also choose to “normalize” τ and x by X_m instead of X ; the choice made here is solely for simplicity. Since the Hamiltonian (5) is a constant for particles inside the phase-space ellipse of the beam core, particles in the core will remain inside the core. For particles outside the core ellipse, the Hamiltonian is time dependent and non-integrable.

Presented in Figs. 1 and 2 are the numerical examples showing that the flutter in $(x, dx/d\tau)$ is reduced in (u, w) . The case studied is an axisymmetric focusing channel with $F(\tau) = \cos \tau$, and $Q^2 = 0.31966$. The betatron phase advance per period for particles inside the matched core is about 90° at zero beam current, and 60° at full beam current (η

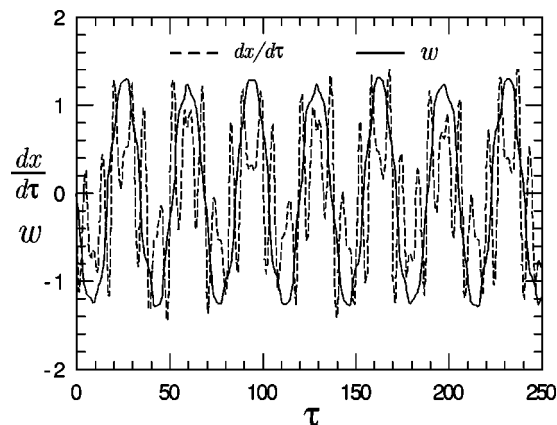


FIG. 2. Velocity $dx/d\tau$ and quantity w of a particle in a mismatched beam propagating in a periodic-focusing channel. The parameter values are described in the text.

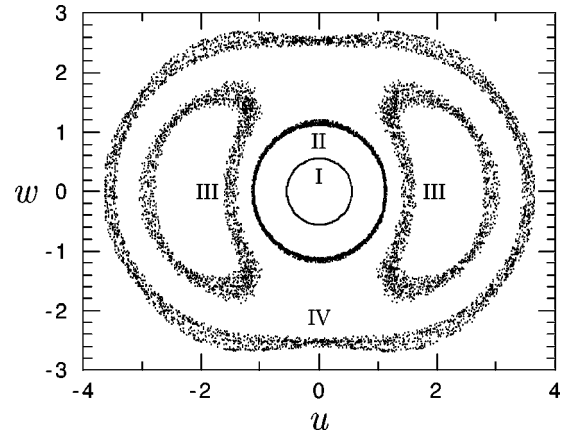


FIG. 3. A stroboscopic plot on the (u, w) phase plane showing four classes of particles discussed in the text.

$= 0.206$). The initial values considered are: $u = 1.3842$, $X = 3.3488$, $u_e = 1/0.9$, $w = dX/d\tau = 0$, and $L_r = 0$.

The approach taken here is to study the dynamics of beam halo in the phase space of (u, w) . Because of the nonlinear parametric driving, the oscillations in u and u_e can be periodic, quasiperiodic, or maybe almost-periodic, depending on the initial conditions and the value of η . Therefore, in making the stroboscopic plots, instead of strobing at a fixed frequency, it is more sensible to strobe at a fixed value of u_e or w_e (e.g., at the local minima where $w_e = 0$) to minimize the shifting in the phase between the strobing and the core oscillation. Numerical results indicate that strobing at a constant period does create a larger spread of points mostly due to the phase shift between the strobing and the envelope oscillation (see Figs. 5 and 7 below). Thus, the stroboscopic plots (plots made from two-dimensional Poincaré maps) proposed here are different from the usual Poincaré plots. These two kinds of plots are the same for uniform-focusing channels where u_e is periodic. In the following, we shall loosely call the relation that links one snapshot to the next the “stroboscopic map.”

At very high beam current, particle motion can become chaotic. One of the deficiencies in projecting a higher-dimension phase-space section onto a two-dimensional plane is the difficulty in detecting the onset of chaotic motion. Another deficiency is that discerning higher-order resonances can be hard or impossible most of the time.

III. GRAPHIC REPRESENTATIONS

Figures 3 and 4 show examples of stroboscopic plots made by strobing at the local minima of u_e for $F(\tau) = (1 + \cos \tau)/2$. The parameter values considered are $L = 0$, $Q^2 = 0.2039$, $\eta = 0.2765$, and $u_e = 0.8$ (initially). For a particle inside the matched core, the phase advance per period (or the tune) is about 120° at zero current and 80° at full beam current. These plots were created by first computing x , $dx/d\tau$, X , $dX/d\tau$, X_m , and $dX_m/d\tau$ simultaneously using Eqs. (1) and (2). The quantities u and w were then calculated using Eq. (4).

At small tune depression, particles can be roughly categorized into five classes according to their motion. Class I particles remain inside the core. Class II particles are outside the phase-space ellipse of the core but not in resonance with the

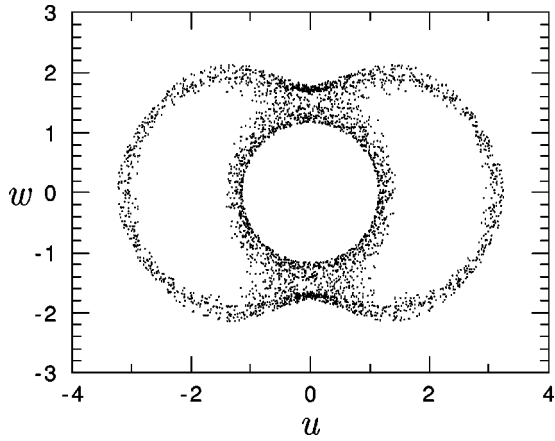


FIG. 4. Stroboscopic plot for a class V particle on the (u, w) phase plane.

core oscillation because they experience less tune depression than the core particles. These particles stay close to the core. Particles in class III oscillate at frequencies near one-half the core oscillation frequency so they can resonate with the core motion to become halo particles. Class IV particles oscillate with large amplitudes and are depressed least in tune so they do not resonate with the core. Figure 3 shows a stroboscopic plot of four particles representing these four classes. The particles in this example start initially from rest with the values of u equal to 0.5551, 1.1203, 1.4281, and 3.4366, for the class I, II, III, and IV particles, respectively. The points of the class II, III and IV particles appear to be scattered near the invariant curves of the Poincaré plots for uniform-focusing channels.

The points of class V particles fall near the separatrices in a Poincaré plot of the uniform-focusing case. Particles in this class can be driven into and out of resonance by the periodic-focusing and the flutter, an effect not found in the uniform-focusing systems and was left out by the smooth approximation in an earlier work [11]. This discovery has a practical implication: since a realistic beam inevitably has some tails instead of a sharp-edged density profile in the transverse direction, in a mismatched beam, some of the particles initially not in resonance with the core oscillation can be driven into the halo region by the mechanism discussed here. Figure 4 is

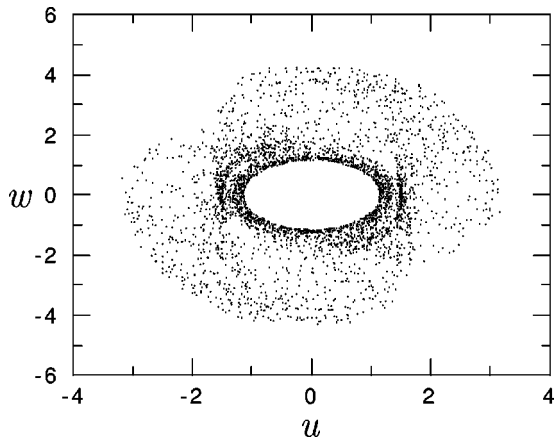


FIG. 5. Shown is a plot on the (u, w) phase plane made by a constant-period strobing for the same particle in Fig. 4.

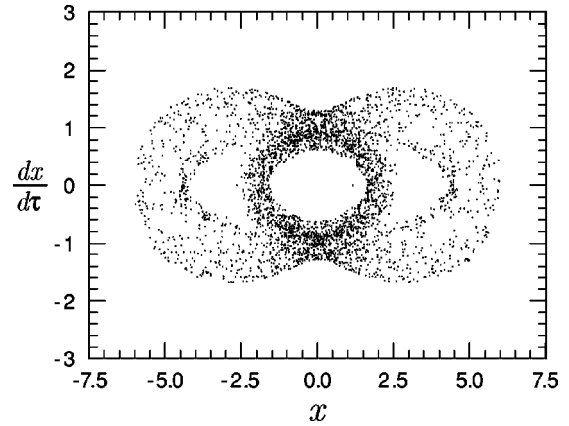


FIG. 6. The stroboscopic plot shown in Fig. 4 is displayed here on the $(x, dx/d\tau)$ phase plane.

a stroboscopic plot for a class V particle with the initial condition $(u, w) \approx (1.1607, 0)$. At large tune depression and strong focusing, the identification of particles' classes becomes ambiguous except for the class I particles.

For comparison, a plot made by strobing at the averaged envelope-oscillation period for the same particle in Fig. 4 is shown in Fig. 5 where we see that points are more scattered and the 2:1 resonance is not apparent. The larger scattering of points in Fig. 5 is mainly due to the phase shift between the strobing and the envelope oscillation as well as the projection. To demonstrate the forte of the proposed method discussed Sec. II, the same plots shown in Figs. 4 and 5 are displayed in Figs. 6 and 7, respectively, on the $(x, dx/d\tau)$ phase planes. Comparing these two sets of plots, especially Fig. 4 with Fig. 7, the advantage of using the variables (u, w) and the ‘‘stroboscopic plot’’ is clear. Note that the 2:1 resonance can be seen in both Figs. 4 and 6.

IV. ANALYTICAL MODEL

The discussion here is a case study aimed to gain qualitative understanding of the halo dynamics. The approach here will follow that in Ref. [5]. We assume the periodic-focusing channel is axisymmetric and the test particle has zero angular momentum. We also limit our discussions to the nonchaotic regime and to the case that the core oscillation is

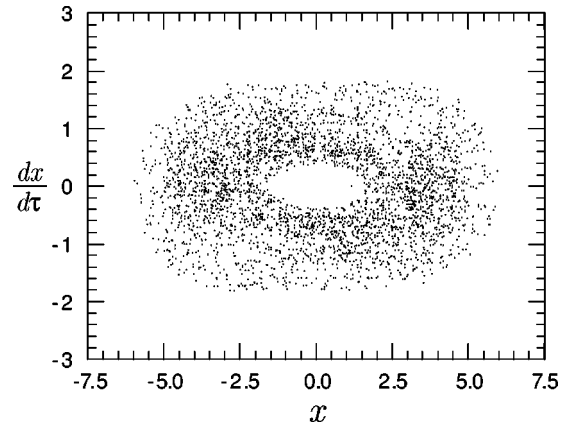


FIG. 7. The stroboscopic plot shown in Fig. 5 is displayed here on the $(x, dx/d\tau)$ phase plane.

not in resonance with the external periodic focusing. Thus, we consider a general form of the lowest-order approximation for the beam envelopes for $F(\tau) = (1 + \cos \tau)/2$, and $F(\tau) = \cos \tau$.

$$X \approx A[1 + a \cos(k't') + b \cos(2t')], \tag{6}$$

where $a \ll 1$ and $b \ll 1$, A is the averaged beam radius, a is the flutter due to the focusing, $k' = 1/f_0$, $t' = f_0 A^2 \psi$; b and f_0 are the amplitude and the half-frequency (in the time variable τ) of the envelope oscillation, respectively. We simplify the problem further by restricting our discussion to a particle outside the beam ellipse and focusing on the case of $k' = n + \delta$ with $\delta \ll 1$. Since the qualitative results for different values of n are similar, we therefore consider the example of $n = 4$ without losing the generality of our conclusions. Assuming the motions of the beam envelope and the particle are near the 2:1 resonance, the polar form of u and w can be written as $u = r \cos(t' - \phi)$, and $w = -r \sin(t' - \phi)$, where the amplitude r and the phase ϕ vary slowly with t' . We then can derive the following equations for r^2 and ϕ :

$$\begin{aligned} \frac{dr^2}{d\psi} &= -2\Theta[r \cos(t' - \phi) - 1] \\ &\quad \times \eta X^2 [1 - r^2 \cos(t' - \phi)] \tan(t' - \phi) \\ &= \frac{\partial(2H_p)}{\partial\phi} \end{aligned} \tag{7}$$

and

$$\begin{aligned} \frac{d\phi}{d\psi} &= f_0 A^2 - 1 + \Theta[r \cos(t' - \phi) - 1] \\ &\quad \times \eta X^2 \left[\frac{1}{r^2} - \cos(t' - \phi) \right] \\ &= f_0 A^2 - \frac{\partial(2H_p)}{\partial r^2}. \end{aligned} \tag{8}$$

Averaging Eqs. (7) and (8) over one resonant particle oscillation period (t' from 0 to 2π) and retaining the zeroth as well as the first-order terms of a and b yield the following equations for particles with $r > 1$:

$$\begin{aligned} \frac{dR^2}{d\psi} &= \frac{\partial(2K)}{\partial\Phi} \\ &= 8a\Gamma \left[\theta_1 + \frac{\lambda}{3} \left(5 - \frac{1}{h} \right) \right] \sin(4\Phi + \delta f_0 A^2 \psi) \\ &\quad - 4b\Gamma [(2-h)\theta_1 + (1+h)\lambda] \sin(2\Phi) \end{aligned} \tag{9}$$

and

$$\begin{aligned} \frac{d\Phi}{d\psi} &= -\frac{\partial(2K)}{\partial R^2} = f_0 A^2 - 1 + \Gamma \left[\left(1 - \frac{1}{h} \right) \theta_1 - \frac{1}{4h^2\lambda} \right] \\ &\quad - \frac{a\Gamma}{12\lambda h^4} (2h^2 - 7h + 2) \cos(4\Phi + \delta f_0 A^2 \psi) \\ &\quad + b\Gamma \left(\theta_1 - \frac{1+h}{8h^3\lambda} \right) \cos(2\Phi), \end{aligned} \tag{10}$$

where R and Φ vary slowly with t' (or ψ), are the averaged values of r and ϕ , respectively, $\Gamma = \eta A^2 / \pi$, $\theta_1 = \cos^{-1}(1/R)$, $h = R^2/2$, $\lambda = \sqrt{R^2 - 1}/R^2$,

$$K(R, \Phi, \psi) = \bar{H}(R, \Phi, \psi) - h f_0 A^2, \tag{11}$$

and

$$\begin{aligned} \bar{H}(R, \Phi, \psi) &= \frac{1}{4\pi} \int_0^{2\pi} [u^2 + w^2 - \eta X^2 \Theta(u-1)(\ln u^2 + 1 - u^2)] dt' \\ &\approx h - \frac{\Gamma}{4} \int_0^{2\pi} [1 + 2a \cos(4t' + \delta t') + 2b \cos(2t')] \Theta[R \cos(t' - \Phi) - 1] \\ &\quad \times [\ln(2h) + 1 - h + \cos(2t' - 2\Phi) + \ln \cos^2(t' - \Phi)] dt' \\ &\approx h + b\Gamma [(2-h)\theta_1 + (1+h)\lambda] \cos(2\Phi) - a\Gamma [\theta_1 + (\lambda/3)(5 - h^{-1})] \\ &\quad \times \cos(4\Phi + \delta f_0 A^2 \psi) + \Gamma \left\{ [\ln(2h) + 1 - h] \theta_1 + h\lambda + \int_0^{\theta_1} \ln(\cos^2 \theta) d\theta \right\} \end{aligned} \tag{12}$$

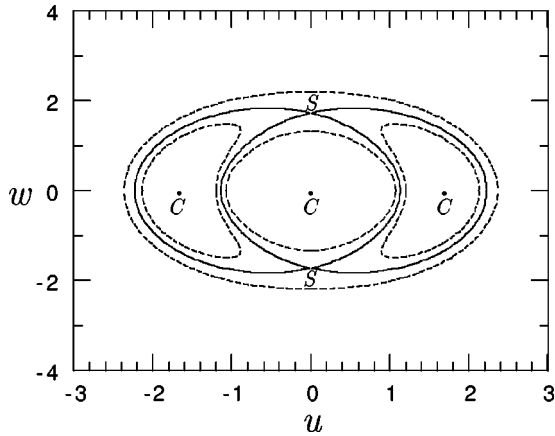


FIG. 8. Examples of the invariants described by Eq. (11) with $a=0$ (constant focusing) for $\eta A^2 = 4.5$ and $b = 0.14$. For the central curve, the separatrix (solid curve), the resonant curve, and the outer curve, the values of K are 0.75, 1.0352, 1.23, and 1.7189, respectively; the values of $f_0 A^2$ are 1.05, 1, 1, and 0.95, respectively. The computation was carried out using Eq. (11) and checked with the solutions of Eqs. (9) and (10).

is the result of averaging the Hamiltonian (5) with $L=0$. In obtaining Eq. (12), the relation $\cos(4t' + \delta t') = \cos(4t' - 4\Phi)\cos(\delta t' + 4\Phi) - \sin(4t' - 4\Phi)\sin(\delta t' + 4\Phi)$ was used and $\delta t' + 4\Phi$ was treated as a slow-varying quantity.

When the focusing is uniform along the z direction, $a = 0$. The quantity K then becomes a constant of motion equivalent to that obtained in Ref. [5] with zero angular momentum. Figure 8 shows some invariants [Eq. (11) with $a=0$], including three stable fixed points (C for centers) and two unstable fixed points (S for saddles) joined by separatrices displayed as solid curves. The phase plane is divided into three types of regions by separatrices: the low-tune region containing the central fixed point, the high-tune region having no fixed point, and the two symmetric half-moon-shape resonant regions each with one stable fixed point. The invariant curves of halo particles fall into the resonant region. External perturbation is needed for particles to cross the separatrices.

In the periodic-focusing case, $a \neq 0$, then K depends on time explicitly; hence there is no well-defined separatrix and no fixed point outside the core area. For $a \ll 1$, Eq. (11) indicates that the points of a stroboscopic map should be scattered near the invariant curves of the uniform-focusing case. An example is given in Fig. 9 to show the smearing of the separatrix and the resonant curves due to the fluctuation described in the averaged Hamiltonian (12). For this figure, the same parameter values used to compute the separatrix in Fig. 8 were considered except for $a=0.05$ and $\delta=0.1677$. Here, a somewhat large value of δ is used to speed up the computation and to make the spread of points more visible. On a stroboscopic plot, we find the class I and II particles' points in the low-tune region, the class III particles' points in the resonant region, and the points of class IV particles in the high-tune region. Note that if $\delta \rightarrow 0$ in Eq. (11), i.e., if the frequencies of the periodic-focusing lattice and the core oscillation become commensurable, it appears that K can be an invariant and Poincaré maps can be constructed by strobing at some common multipliers of the frequencies as discussed in Ref. [11]. However, in this situation, the stability of the

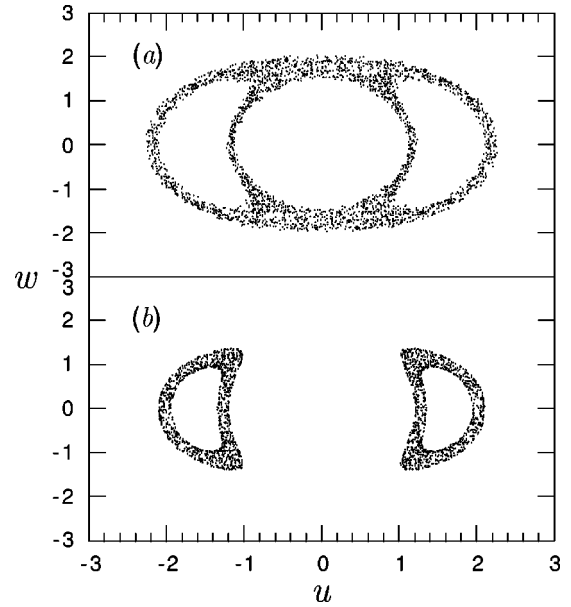


FIG. 9. Shown is the smearing of the separatrix (a) and the resonant curves (b) due to the fluctuation described in the averaged Hamiltonian (12). Points were obtained by numerically solving Eqs. (9) and (10). The same parameter values used to compute the separatrix in Fig. 8 were considered here except for $a=0.05$ and $\delta = 0.1677$. The initial values used are $(u, w) = (2.13, 0)$ for (a), and $(u, w) = (1.95, 0)$ for (b).

envelope oscillation and the validity of Eq. (6) should be checked first to see if such an approach is feasible. Also, when comparing the result in Eq. (11) with the numerical solutions of Eqs. (1) and (2), we should keep in mind that the model envelope in Eq. (6), at best, is only an approximation to some solutions of the nonlinear envelope equation. For nonzero beam currents, numerical search for a mismatched core oscillation with a frequency at a subharmonic of the focusing frequency using Eq. (1) is being pursued.

V. APPLICATION TO QUADRUPOLE-FOCUSING SYSTEMS

For quadrupole-focusing systems, the equations for the beam envelope and particle motion in the x direction are

$$\frac{d^2 X}{d\tau^2} + Q^2 X F(\tau) - \frac{2\hat{\eta}}{X+Y} - \frac{\epsilon_x^2}{X^3} = 0, \quad (13)$$

and

$$\frac{d^2 x}{d\tau^2} + Q^2 x F(\tau) = \frac{2\hat{\eta}x}{\Xi_x(\Xi_x + \Xi_y)}, \quad (14)$$

respectively, where $X = X_r \sqrt{k}$, $Y = Y_r \sqrt{k}$, X_r and Y_r are the beam envelopes in the x and y directions, respectively, $x = x_r \sqrt{k}$, x_r is the displacement of the beam particle in the x direction from the beam axis, $\hat{\eta} = qI / (2\pi\epsilon_0 m_0 \gamma^3 v^3 k)$, ϵ_x is the beam emittance in the x direction, $\Xi_x = (X^2 + \xi)^{1/2}$, and $\Xi_y = (Y^2 + \xi)^{1/2}$. The value of ξ is zero when the particle is inside the beam, and is given by the solution of the equation $(x/\Xi_x)^2 + (y/\Xi_y)^2 = 1$ when the particle is outside the beam, where $y = y_r \sqrt{k}$, and y_r is the excursion of the beam particle

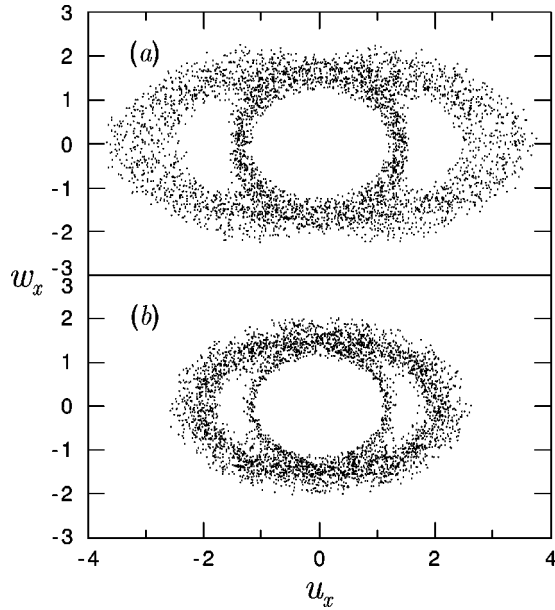


FIG. 10. Stroboscopic plot showing the resonance of a halo particle with (a) the breathing mode and (b) the quadrupole mode oscillations of the beam envelope in a quadrupole-focusing channel.

in the y direction from the beam axis. The equations for the beam envelope and particle motion in the y direction are similar.

Due to a lack of good guidance to the global phase-space structure of this kind of dynamic system, attempts in making two-dimensional plots, i.e., Poincaré or “stroboscopic” plots, have only very limited success. It is found that for a particle having nonzero angular momentum, even a small amount, the points on the plot are totally dispersed. It appears that two-dimensional plots, except for some special cases, do not seem to provide insightful displays of the global system behavior. Thus, to deal with a problem of two degrees of freedom like this, it is necessary to consider the x and y motion of the particle separately by setting one of the coordinates to zero, e.g., $y=0$ and $dy/d\tau=0$. The method developed for the axisymmetric systems can be generalized here by using the variables defined according to $u_x = x/X$, $w_x = X(dx/d\tau) - x(dX/d\tau)$, $u_{ex} = X_m/X$, $w_{ex} = X(dX_m/d\tau) - X_m(dX/d\tau)$, and by using similar definitions for the y -direction variables.

We consider the case for which the envelope oscillations are close to one of the eigenmodes of the linearized envelope equations: the usual breathing mode with X and Y oscillating in phase, and the quadrupole mode with X and Y oscillating at 180° off phase. Particles may interact with either one of these two envelope modes, or a combination of them to move into beam halo [11]. Examples of stroboscopic plots for particles in resonance with these two modes of the envelope oscillation are shown in Fig. 10 for $F(\tau) = \cos(\tau)$, $\epsilon_x = \epsilon_y = 1$, $Q^2 = 3.198$, and $\hat{\eta}/\epsilon = 0.2502$. These parameter values correspond to a tune depression from 90° to 70° for particles inside the matched beam. The initial conditions used are $w_{ex} = w_{ey} = w_x = u_y = w_y = 0$ and $u_{ex} = u_{ey} = 0.8$, $u_x \approx 1.1922$ for (a); $u_{ex} = 0.85$, $u_{ey} = 1.15$, $u_x \approx 1.0947$ for (b).

VI. CONCLUSIONS

A method has been developed to use the particle-core model for studying the dynamics of halo particles in a mismatched continuous beam propagating through an axisymmetric periodic-focusing channel. It was assumed that the beam-particle density and envelope are described by the KV distribution function and envelope equation. A canonical transformation and a technique of strobing were proposed to reduce, in the new variables, the fluctuation due to the periodic focusing. This approach allows one to perceive the dynamics of halo particles through the stroboscopic plots. The method is applicable to a wide range of parameter values without using any smooth approximation, and is not limited by the constraint that the frequency of core oscillation need be commensurable with that of the transverse focusing. Numerical examples were given for illustration and an analytical model was discussed to assist the understanding of halo formation.

Using this method, we learned that the parametric resonance, like the one studied in the uniform-focusing case, is still the major mechanism to cause the large-amplitude oscillation of halo particles. We also learned that certain particles with initial oscillation amplitudes slightly larger than the core radius, but not in the halo region, can be brought into resonance with the core oscillation by the fluctuation of the periodic focusing. Since the transverse density profile of a realistic beam inevitably has some tails instead of a sharp-edged distribution, some particles in the tails of a mismatched beam can be driven into halo by the mechanism discovered here. Previous particle-core studies of halo formation in the uniform-focusing channel found the existence of a separatrix between the core and the resonant region, and concluded that either the halo particles were initially in the resonant region [5,12] or the halo particles were brought across the separatrix from the core by some kind of process like coherent instability [15]. For periodic-focusing channels, the mechanism discussed in this present work adds another possible process of halo formation.

Application of this method to a quadrupole-focusing system was also studied. It was discussed that for a problem of two degrees of freedom in the particle-core model, two-dimensional plots can be easily understood only for particles having zero or almost zero angular momentum. In that case, the x and y motion of particles can be treated separately and it was found that particles may resonate with either the breathing mode or the quadrupole mode of the envelope oscillation, or a combination of these two modes, to move into beam halo.

ACKNOWLEDGMENTS

This work was supported by Los Alamos National Laboratory, under the auspices of the U.S. Department of Energy. The author would like to thank Dr. A. Jason and Dr. T. Wangler for their comments and suggestions.

- [1] R. Jameson, Los Alamos National Laboratory Report No. LA-UR-93-1209, 1993.
- [2] J. S. O'Connell, T. P. Wangler, R. S. Mills, and K. R. Crandall, *Proceedings of the 1993 Particle Accelerator Conference, Washington D.C., 1993*, edited by S. T. Cornellussen (IEEE, Piscataway, NJ, 1993), p. 3657.
- [3] T. P. Wangler, Los Alamos National Laboratory Report No. LA-UR-94-1135, 1994.
- [4] J. Lagniel, Nucl. Instrum. Methods Phys. Res. A **345**, 46 (1994); **345**, 405 (1994).
- [5] R. Gluckstern, Phys. Rev. Lett. **73**, 1247 (1994).
- [6] C. Chen and R. C. Davidson, Phys. Rev. Lett. **72**, 2195 (1994); Phys. Rev. E **49**, 5679 (1994).
- [7] S. Y. Lee and A. Riabko, Phys. Rev. E **51**, 1609 (1995).
- [8] C. Chen and R.A. Jameson, Phys. Rev. E **52**, 3074 (1995).
- [9] T. P. Wangler, R. W. Garnett, E. R. Gray, R. D. Ryne, and T.-S. Wang, *Proceedings of the XVIII International Linear Accelerator Conference, Geneva, 1996*, edited by C. Hill and M. Vretenar (CERN Report No. CERN 96-07, 1996), p. 372.
- [10] H. Okamoto and M. Ikegami, Phys. Rev. E **55**, 4694 (1997).
- [11] M. Ikegami, Phys. Rev. E **59**, 2330 (1999); M. Ikegami and M. Mitzumoto, Argonne National Laboratory Report No. ANL-98/28, 1998, edited by C. E. Eyberger, R. C. Pardo, and M. M. White, p. 821.
- [12] T. P. Wangler, K. R. Crandall, R. Ryan, and T.-S. Wang, Phys. Rev. ST Accel. Beams **1**, (1998).
- [13] See, for example, S. Wiggins, *Global Bifurcations and Chaos: Analytical Methods* (Springer-Verlag, New York, 1988), Sec. 4.2 for discussions on multifrequency parametrically forced systems.
- [14] I. M. Kapchinskij and V. V. Vladimirkij, in *Proceedings of the 2nd International Conference on High Energy Accelerators* (CERN, Geneva, 1959), p. 274.
- [15] R. L. Gluckstern, W.-H. Cheng, and H. Ye, Phys. Rev. Lett. **75**, 2835 (1995).